Large-Area Metasurface Perfect Absorbers from Visible to Near-Infrared

*Gleb M. Akselrod, Jiani Huang, Thang B. Hoang, Patrick T. Bowen, Logan Su, David R. Smith, and Maiken H. Mikkelsen**

Absorption of light is central to the operation of devices such as photovoltaics,[1] photodetectors,[2] imaging sensors,[3] controlled-emissivity surfaces,[4] and biosensors.[5] Naturally occurring materials either have weak absorption or produce strong reflections, and have poorly defined spectral features beyond the visible spectrum.[6] Nearly perfect absorbers based on metasurfaces with metallic elements[7] have been developed to address these limitations in spectral ranges from the near-infrared[5,8] to microwave.[9] However, each metasurface element must be deeply subwavelength in size, requiring the use of top-down lithography techniques,[8] inherently limiting their scalability to large areas and for visible spectrum response. In this work, we demonstrate large-area metasurfaces with nearly perfect absorption (99.7%) over truly macroscopic areas using a simple, scalable, and conformal solution-based assembly technique. The metasurface elements are composed of colloidally synthesized silver nanocubes coupled to a metal film. The resonance wavelength is easily tunable from the visible to the near-infrared spectrum, with the absorbers showing good performance at oblique angles. Given their broad tunability, high efficiency, and good spectral selectivity over a large spectral range, these metasurface absorbers can be integrated with existing technologies for enhanced photodetectors and imaging devices, and for enhanced photocatalysis.[10] The conformal, solution-based deposition also could enable control of absorption and emissivity of surfaces of arbitrary geometry and size.

Organic dyes and inorganic pigments have been used as color-selective absorbers of visible light throughout human history for paints, inks, clothing, and food. However, the properties of these naturally occurring materials as light absorbers are insufficient for many modern photonics applications. Natural materials derive their strong absorption from their electronic response, which often coincides with large values of relative electric permittivity (ε) and values of relative magnetic permeability (μ) near unity. The large difference between ε and μ translates to a large impedance $z = \sqrt{\mu/\varepsilon}$ mismatch between the material and free space, leading to strong reflections. Furthermore, absorbing materials at wavelengths above 1000 nm have broadband and not spectrally selective absorption due to a reliance on photon absorption or materials with small bandgaps.[6]

The limitations associated with natural materials can be addressed by creating materials structured on a length scale larger than a molecule but much smaller than the wavelength of light. For example, to reduce reflection and increase absorption, surfaces can be created with a low effective refractive index using forests of carbon nanotubes[11] or porous metal,[12] or with a graded refractive index using microstructured silicon.[13] However, these approaches result in spectrally broad absorption across the visible and near-infrared. For applications such as hyperspectral imaging, emissivity control, and for surfaces with a tailored absorption spectrum, narrowband absorption is essential.[4] Interference effects in absorbing materials have also been utilized, but these structures show incomplete absorption and strong angle-dependence.[14]

Absorbing surfaces that are both spectrally selective and eliminate reflection can be created by deliberately engineering subwavelength elements that act as resonators.[9,15,16] Arrays of such resonator elements collectively act as a metasurface,[17–20] with an effective electric and magnetic response that creates impedance matching to free space and hence complete absorption at the resonant wavelength.[9,21] The geometry of each subwavelength element and their spatial arrangement determines both the resonant wavelength and the effective impedance of the surface.

A common absorber design consists of a metallic subwavelength element such as a disk or a metamaterial resonator situated over a metallic ground plane. Such metasurface absorbers were first proposed and demonstrated in the microwave spectral region.[9] In the visible and infrared spectral ranges, high-resolution photolithography, electron beam lithography,[22] or ion beam milling[23] is needed because individual resonators must be $\approx\lambda/10$ in size, where λ is the wavelength of light. The need for top-down lithographic patterning inherently limits the scalability and commercialization potential of metasurface absorbers. Even with the parallel nature of high-resolution photolithography, colloidal etching lithography,[24] or nanosphere templating,[20] the absorbers are limited to planar wafers and cannot be fabricated on conformal surfaces and on meter

Dr. G. M. Akselrod, J. Huang, Dr. T. B. Hoang, P. T. Bowen, L. Su, Prof. D. R. Smith, Prof. M. H. Mikkelsen
Center for Metamaterials and Integrated Plasmonics
Duke University
Durham, NC 27708, USA
E-mail: m.mikkelsen@duke.edu

Dr. G. M. Akselrod, P. T. Bowen, Prof. D. R. Smith, Prof. M. H. Mikkelsen
Department of Electrical and Computer Engineering
Duke University
Durham, NC 27708, USA

J. Huang, Dr. T. B. Hoang, Prof. D. R. Smith, Prof. M. H. Mikkelsen
Department of Physics
Duke University
Durham, NC 27708, USA

DOI: 10.1002/adma.201503281

length scales. Self-assembled metal islands coupled to a metal film have been demonstrated as metasurface absorbers,[25–27] but this approach leads to broad resonances and limited wavelength tunability. Since the absorber concept does not rely on exact periodicity, the use of metal nanocubes coupled to a metal film was proposed as a scalable, colloidal approach to coating large area surfaces; however, initial experimental demonstrations showed poor absorption and limited spectral tunability.[21] Recently, Rozin et al. demonstrated metasurface absorbers based on metal–film-coupled nanocubes with resonances from the near- to mid-IR.[31] To date, large-area and spectrally selective perfect absorbers have not been demonstrated in the visible spectrum.

Here we demonstrate nearly perfect absorbers over large areas on conformal surfaces, and without any lithographic processing, with spectral tunability from the visible to near-infrared spectrum. The absorbers are based on colloidally synthesized silver nanocubes situated over a metal film (**Figure 1**a), separated by well-controlled nanoscale spacer. Each film-coupled nanocube acts like a magnetic dipole,[28] where the resonance of the dipole is determined by the size of the nanocube and the spacer.[29] The collective action of many nanocubes on the surface creates an effective magnetic response. As a result, the impedance of the surface is matched to free space and both reflection and transmission of the surface are eliminated, resulting in complete absorption.[21] The incident light is dissipated by the generation and decay of surface plasmons in the gap between the bottom nanocube facet and the top of the metal film.

The assembly of the absorbers is straightforward and inherently large-area and conformal (Experimental Section). Briefly, the process begins by chemical synthesis of silver nanocubes following a well-established process.[30] To form the metasurface, a thin metal film of 50–100 nm is first deposited on the desired substrate. In most experiments presented in this work, evaporated gold is used as the ground plane. However, other plasmonic metals such as silver and aluminum can be used as well as large-area deposition methods such as electroplating. The nanoscale spacer (<10 nm) layer is deposited on the metal film using layer-by-layer dip coating of alternating cationic and anionic polymers, with each layer ≈1 nm in thickness. The dip coating method creates nanometer precision spacers over macroscopic areas using a simple solution-based process. Finally, the substrate is dip-coated or exposed to a solution of the negatively charged silver nanocubes, which adhere to the positively charged top polymer layer. Due to this robust immersion-based fabrication method, the optical properties are not sensitive to precise fabrication conditions as can be the case with Langmuir–Blodgett deposition.[31] A small region of the metasurface is shown in the angled scanning electron micrograph (SEM) in Figure 1a.

Figure 1b shows the reflection spectrum from a metasurface absorber with a resonance in the visible spectrum at 650 nm, obtained using a combination of 75-nm nanocubes and a 7 nm spacer layer. Using a surface coverage density of 15%, we obtain a minimum reflectivity of 0.4% at the resonance wavelength. These measurements were done at a near-normal incidence angle of $\theta_{inc} = 6°$, to avoid using a beamsplitter. To visually demonstrate the nearly complete absorption, an absorber area with a 10 mm diameter is illuminated at near-normal incidence by a defocused laser spot slightly larger than the absorber region (Figure 1c). Figure 1d shows the reflection from the sample imaged onto a screen as the laser wavelength is swept from 500 to 700 nm. When the laser wavelength is at the absorption peak at $\lambda = 650$ nm, the 10 mm metasurface area appears completely black relative to the reflection from the gold film around the absorber.

To determine the fraction of nonreflected light that is scattered instead of absorbed, the scattered light was measured using a goniometer setup that collects light at angles outside the incidence angle of $\theta_{inc} = 6°$. This measurement technique was chosen because it provides not only the total scattered power as

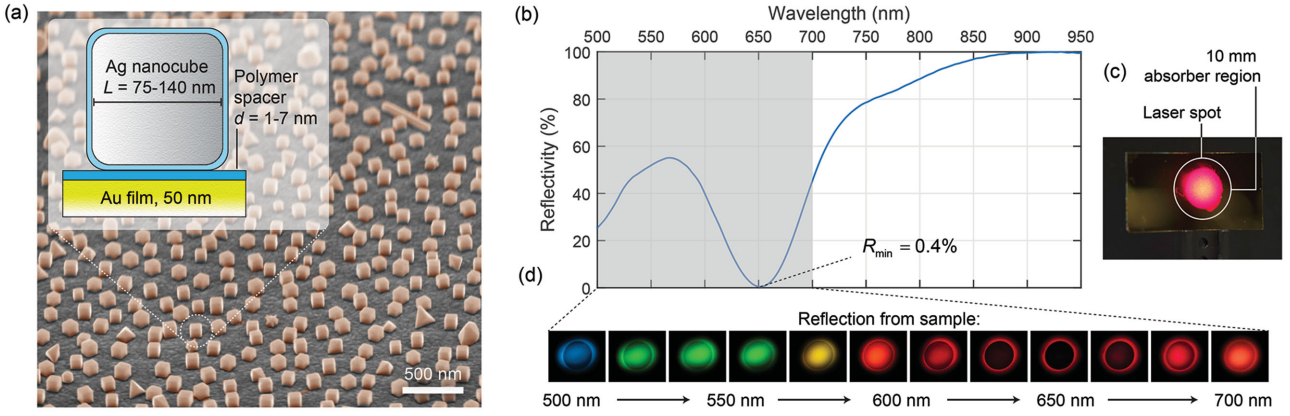

Figure 1. Metasurface perfect absorber based on colloidal silver nanocubes. a) SEM image of perfect absorber surface consisting of a gold film covered with silver nanocubes. Inset shows cross-section of single subwavelength resonator, in which the gap thickness is controlled by a 1–7 nm polymer layer. b) Reflection spectrum from an absorber with a resonance at 650 nm, utilizing 75 nm nanocubes and a 7 nm spacer, showing a minimum reflectivity of 0.4%. c) Image of sample with a 10 mm region coated with nanocubes on top of gold, while surrounding region is coated only with gold. A defocused laser with a diameter of ≈13 mm illuminates the absorber region. d) Images of the laser beam on a screen after reflection from the absorber sample shown in (c), as the laser wavelength is swept from 500 to 700 nm. When the laser is resonant with the absorption at 650 nm, no reflection is seen from the nanocube coated region.

Adv. Mater. **2015**,
DOI: 10.1002/adma.201503281

can be obtained from an integrating sphere measurement, but also angle-resolved scattering information. When integrated over the entire half-sphere of observation, the scattered light was found to be <1% of the incident power, showing that the lage on-resonance extinction is primarily due to absorption (see the discussion and Figure S4 in the Supporting Information). In particular, for the absorber shown in Figure 1b, given the ≈1% scattering and 0.4% reflection, 98.6% of light at near normal incidence and at the plasmon resonance wavelength is absorbed. This small amount of scattering, which is observed both on-resonance and off-resonance, is attributed to silver particles other than nanocubes, which can have a broadband scattering spectrum. As determined from SEM imaging (Figure 1a), ≈91% of the particles in our fabricated samples are nanocubes with a tight size distribution (Figure S3 in the Supporting Information), while residual particles are pyramids, rods, and other shapes. With better nanocube purification, the metasurface performance could be even further improved.

The absorption phenomena of the nanocubes can be modeled analytically by treating the nanocubes as a metasurface with a magnetic susceptibility that is placed over a gold film (Figure S1 in the Supporting Information).[21] The magnetic susceptibility of the metasurface arises from an effective magnetic dipole moment that is created by the fundamental resonance of each cube. The polarizability of each individual nanocube can be found analytically using a form of temporal coupled mode theory, which has recently been used to analyze the resonances of the nanocubes.[28] Provided that the separation between the cubes is sufficiently subwavelength, the lattice of polarizable nanocubes can be homogenized to form an effective magnetic metasurface that sits over the metal film. Absorption occurs when the reflected wave that is generated by the electric surface currents in the film cancel the wave generated by the magnetic surface currents in the metasurface. This theory correctly predicts the perfect absorption and resonance wavelength of the metasurfaces (Figure S2 in the Supporting Information).

Since reflection and scattering from the surface is suppressed, the incident light at the resonance wavelength is dissipated by decaying plasmons. The spacer layer between the nanocube and the gold film is a dielectric which is completely transparent at visible and near IR wavelengths. Consequently, the observed absorption is due exclusively to the decay of plasmons in the silver nanocube and the gold film. Due to the symmetry of the gap plasmon mode, the fields in the nanocube and gold film are roughly equal,[29] resulting in approximately equal dissipation in both metals. In the absence of radiative decay, as is the case in our system, the decay of the gap plasmons at visible and near IR frequencies occurs by the process of Landau damping. In this process, the energy of the collective electron oscillation is transferred to a single excited (hot) electron on a time scale of 1–100 fs.[32,33] Some of these hot electrons could be collected as photocurrent by integrating semiconductors into the gap region or used for photocatalysis.[32] The hot electron collection efficiency depends on their energy and momentum distribution, which in turn is determined by the electronic structure of the metal, the geometry of the structure, and momentum of the initial plasmon, among other factors.[34] In the absence of hot electron collection, these excited electrons eventually couple to phonons in the metal, generating heat, which itself could be harnessed for controlled emissivity surfaces and thermal photovoltaics.

The resonance of the absorber can be tuned from the visible (650 nm) to the near-infrared spectrum (1420 nm) by using different nanocube sizes and by controlling the spacer thickness, thereby changing the resonant cavity formed between the nanocube and metal film (**Figure 2**). For this work, silver

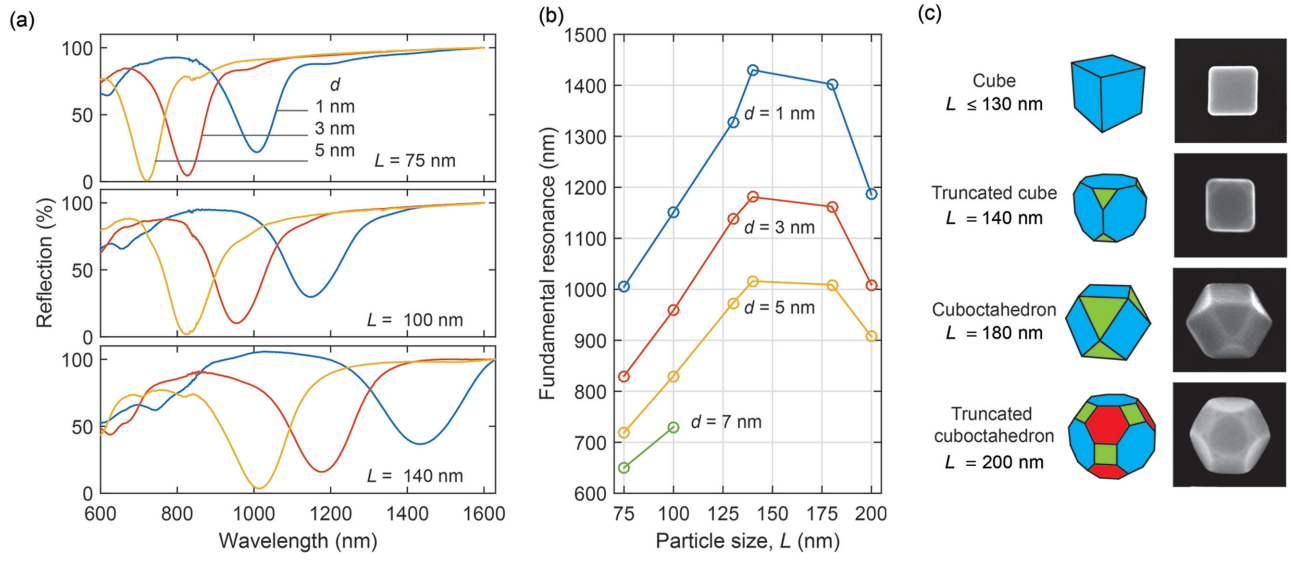

Figure 2. Tuning the absorber resonance from visible to near-infrared. a) Reflection spectra of absorbers with resonances from the visible to the near-infrared using a range of nanocube sizes (*L*) and spacer layer thicknesses (*d*). b) Resonance wavelength as a function of particle size and spacer thickness. c) SEM images of typical particles from each synthesis having average particle size *L*. For $L \geq 140$ nm the particles become noncubic, transitioning to a truncated cube, to a cuboctahedron, to a truncated cuboctahedron. As the particle size increases, the facets become smaller, blueshifting the absorber resonance, seen in (b).

nanocubes were synthesized and supplied by nanoComposix, Inc. (San Diego). The average nanocube size can be tailored from L = 75–140 nm by controlling the synthesis parameters, resulting in excellent control of the resonance wavelength. The spectral selectivity of the absorbers, with a linewidth of ≈100 nm, is enabled by the narrow nanocube size distribution, which is achieved during colloidal synthesis (Figure S3 in the Supporting Information). With increasing size, the silver particles develop new facets, becoming noncubic for particle sizes $L \geq 140$ nm (Figure 2c). As a result, while the size of the particles increases, the individual facets become smaller, reducing the resonator size and blueshifting the resonance (Figure 2b). The polymer spacer layer thickness is controlled with ≈2 nm increments from 1 to 7 nm using the dip coating method. For gap thickness >10 nm, the resonance monotonically approaches the uncoupled nanocube resonance.[35] The resonance of the samples was found to blueshift slightly after 1–2 days in air due to oxidation of the silver nanocubes. However, optical properties were found to be stable for months if the samples were stored in vacuum between experiments. Similar protection could be provided by a deeply subwavelength polymer encapsulation layer that is conformal to the nanocubes, which would minimize reflections. Additionally, silver nanocubes could be replaced with gold nanocubes, which can be synthesized with good size uniformity.[36]

In addition to nanoscale control of the resonator dimensions, we demonstrate fine control over the surface density of the nanocubes, and hence, the optical properties. The nanocube density is controlled by the time the substrate is exposed to the nanocube solution (**Figure 3**). In this demonstration, the nanocube surface fill fraction is tuned from 5.3% to 19.2% over a centimeter scale sample. The darkfield microscopy images of each sample show a color change as the λ = 790 nm resonance increases in strength with increasing nanocube density, as seen in the corresponding SEM image (Figure 3b). The maximum absorption at the resonance wavelength correspondingly increases to 99.7% at a surface coverage density of 19.2%, which is equivalent to a mean spacing between nanocubes of l = 228 nm (Figure 3c). Despite the solution based deposition method, the nanocube spatial distribution shows local periodicity over ≈400 nm due to nanocube repulsion, as was determined by analyzing the radial distribution function of nanocube positions (Figure S4 in the Supporting Information). At longer distances, no spatial order is observed.

For longer deposition times, the fill fraction remained almost unchanged, indicating that repulsion between adhered nanocubes and dissolved nanocubes occurs at distances larger than the silver boundaries. This could be due to extended polymer chains of poly(vinyl pyrrolidone) attached to the nanocube surface, which remains after synthesis.[37] Larger fill fractions could be obtained by modifying the nanocube ligands or using other deposition techniques such as Langmuir–Blodgett.[31] The relatively low fill fraction needed to achieve nearly perfect absorption at a single wavelength suggests the possibility of using multiple species of nanocube sizes to obtain tailored and multiresonant absorption spectra.[4]

In contrast to metasurface absorbers fabricated using lithography, the nanocube perfect absorbers can be assembled over surfaces of arbitrary size and shape. **Figure 4**a shows a 5 cm diameter wafer coated with the perfect absorber. Under resonant illumination at λ = 645 nm, the wafer shows almost no visible reflection, in contrast to the same wafer coated only with gold. The red hue visible on the coated wafer (Figure 4a) is due to a small amount of residual scattering from the nanocubes and larger noncubic particles. The scattered power was measured to be <1% of the incident power on resonance, as discussed above (Figure S5 in Supporting Information) and can likely be suppressed with improved nanocube purification. For comparison, a 5 cm diameter wafer coated only with a gold film shows strong reflection of the same laser beam.

The absorber can also be coated on arbitrary curved surfaces. A metasurface absorber was assembled conformally from solution over the entire surface of a glass half-sphere, 2.5 cm in diameter, with silver serving as the ground plane material

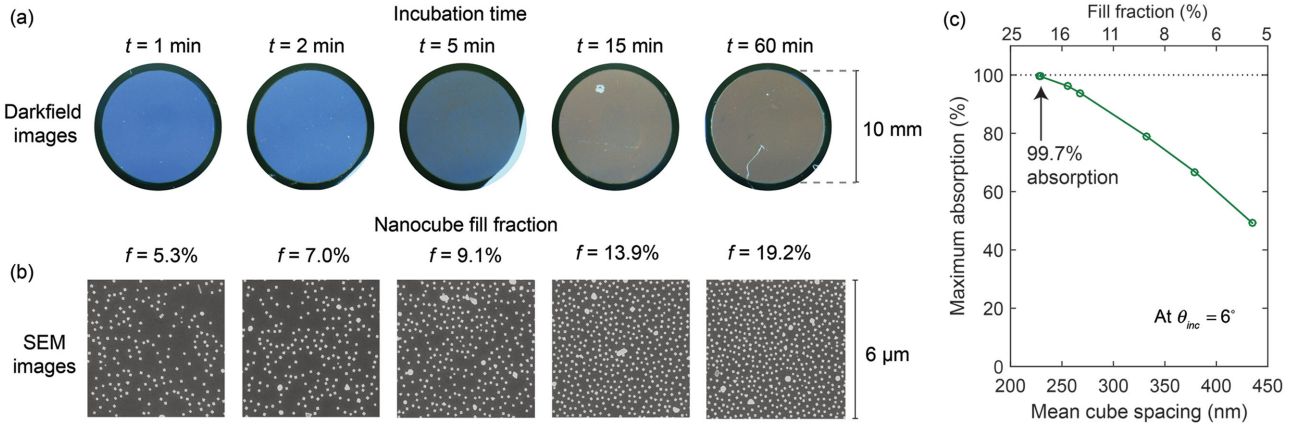

Figure 3. Controlled nanocube density. a) Darkfield microscopy images of a 10 mm absorber region with increasing density of 100 nm nanocubes, from an area fill fraction of f = 5.3% to 19.2%. The density is controlled by the time, t, that the sample is exposed to the nanocube solution. b) SEM images of the samples in (a) showing increasing nanocube density. c) Absorption at the resonance wavelength of 790 nm as a function of nanocube fill fraction, and also plotted versus mean nanocube separation, at an incidence angle θ_{inc} = 6°. The maximum absorption is 99.7% at a fill fraction of 19.2% (228 nm mean cube spacing).

Adv. Mater. 2015,
DOI: 10.1002/adma.201503281

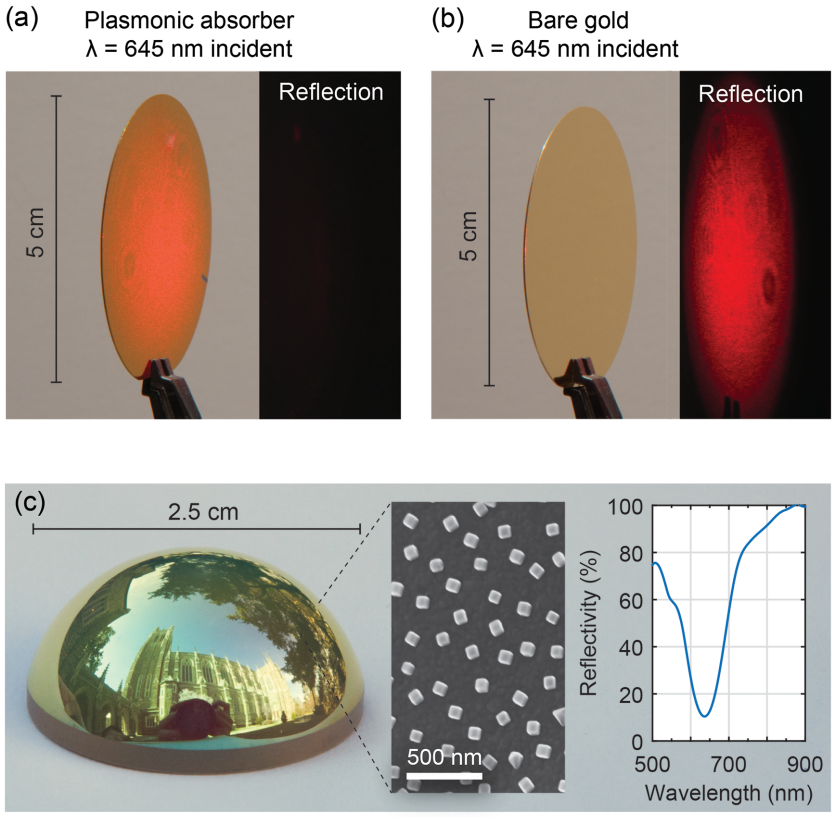

Figure 4. Large area and conformal absorber. a) A 5 cm diameter wafer coated over the entire surface with a gold film, a 7 nm spacer, and 75 nm nanocubes, with a resonance of 645 nm. A defocused 645 nm laser beam is incident on the sample and the reflection is imaged on a screen, showing almost no visible reflection. b) For comparison with (a), a 5 cm wafer coated only with a gold film shows strong reflection of the laser beam, imaged using the same camera exposure settings. c) A glass half-sphere coated with 100 nm of silver and a 7 nm polymer spacer layer, followed by conformal deposition of 75 nm nanocubes. Insets show SEM image taken on the side slope of the sample, and the near-normal incidence reflectance spectrum.

(Figure 4c). The green tint to the reflection of the objects in the surroundings occurs because the red wavelengths are absorbed by the metasurface. The inset shows an SEM image of a ≈1 μm region of the half-sphere, demonstrating how this macroscopic object derives its optical properties from precisely engineered optical elements at the nanoscale. The reflectivity of the surface shows absorption at the resonant wavelength ($\lambda = 635$ nm) of 90%, which is only limited by the solution deposition time and in principle can approach the nearly perfect absorption seen in Figure 1 by obtaining a higher nanocube surface density.

The metasurface presented in this paper is qualitatively similar to the approach of Rozin et al. in that both studies rely on film-coupled silver nanocube as the metasurface element.[31] However, in their work the metasurface elements are arranged at a very high density using Langmuir–Blodgett deposition, resulting in near-field coupling between the elements. This coupling delocalizes the plasmon mode over several film-coupled nanocubes, which redshifts the resonance to mid IR wavelengths. In turn, this reliance on near-field coupling makes this approach sensitive to fabrication conditions that affect the nanocube spacing and hence the resonance wavelength. Furthermore, Langmuir–Blodgett deposition may be difficult to scale to surfaces with arbitrary shape. In contrast, our simple dip coating approach is both highly robust and insensitive to exact fabrication conditions and is scalable to surfaces with arbitrary size or shape. In addition, not relying on near-field coupling between nanocubes allows us to achieve resonances at visible wavelengths.

In many applications such as thermal photovoltaics, photodetection, and emissivity control, complete absorption must be accomplished at normal as well as oblique incidence and the absorbing surface must be insensitive to polarization. In **Figure 5**a, we visualize the absorption at oblique angles of a 10 mm absorber area with a resonance in the visible at $\lambda = 650$ nm. The metasurface shows nearly complete absorption at incidence angles up to 50°. The angular behavior of the absorbers is quantified using white light reflectance measurements as a function of angle (Figure 5b,c) (Experimental Section). The reflection spectrum for a sample with a resonance at 790 nm and a 19.2% nanocube fill fraction is nearly angle-insensitive for incidence angles less than 50° (Figure 5b). The absorption resonance for transverse electric polarized light shows a slight redshift with increasing angle ($\Delta\lambda = 15$ nm at $\theta_{inc} = 50°$), while the spectrum for transverse magnetic light shows a slight blueshift ($\Delta\lambda = -6$ nm at $\theta_{inc} = 50°$). The on-resonance absorption and its angular dependence can be tuned by changing the nanocube density from 5.3% to 19.2% using the controlled deposition method (Figure 5c). For a fill fraction of 19.2%, the maximum absorption at $\theta_{inc} = 6°$ is 99.7% and remains above 95% absorption as the incidence angle is increased to 50°. The angular dependence of the on-resonance absorption is found to be completely independent of incident polarization (Figure S6 in the Supporting Information).

The metasurfaces based on colloidal nanocubes are nearly perfect absorbers that can be fabricated over truly macroscopic areas and on arbitrary surfaces using simple solution-based deposition techniques. These absorbers are spectrally selective, with a tunable resonance from visible to near-infrared wavelengths. The optical properties of these macroscopic metasurfaces are derived from the controlled nanoscale structure of the individual film-coupled nanocube elements. The spectrally tunable absorption and large-area fabrication suggests the possibility of directly integrating these metasurfaces with existing technologies for imaging and photodetection. The strong plasmon confinement in the nanoscale gaps could also be harnessed for photocatalysis applications such as water splitting.[10] The resonances could be moved deeper into the infrared spectrum by utilizing larger colloidal nanoparticles with larger metallic facets. Furthermore, the

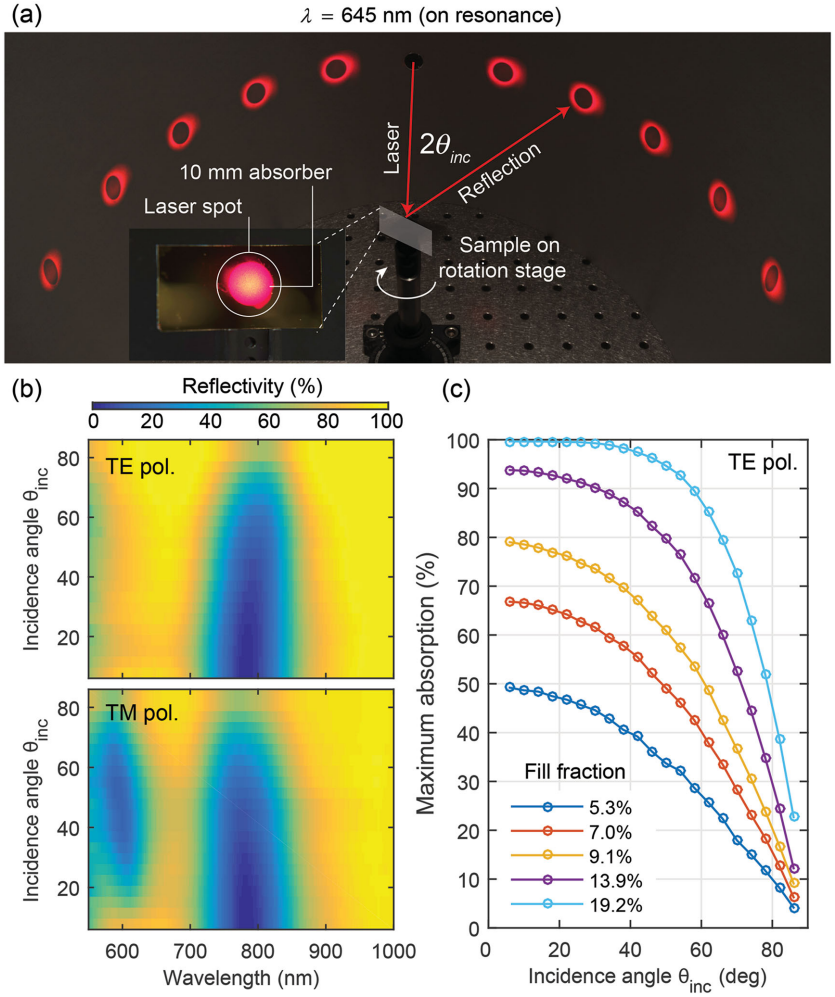

Figure 5. Absorption behavior with angle and polarization. a) Reflection of a defocused laser beam from a 10 mm absorber is imaged on a screen. Laser wavelength is 645 nm, which is resonant with the absorber. The image is an overlay of single exposures at each incidence angle θ_{inc} from −50 to 50° in 10° increments. Almost complete absorption is seen at all angles in the region on the sample covered by nanocubes. b) Reflection spectrum as a function of incidence angle from a sample with a 790 nm resonance, under transverse electric and transverse magnetic incident polarization. c) Absorption at the resonance wavelength as a function of incidence angle for samples with varying fill fraction from $f = 5.3\%$ to 19.2%.

low coverage density required for perfect absorption suggests the possibility of creating absorbers with tailored spectra by combining multiple nanocube sizes. These metasurfaces could also function as active devices, for example, by integrating a semiconductor into the nanocube-film gap region and collecting the hot electrons which are generated in the metals.[32]

Experimental Section

Sample Fabrication: With the exception of conformal coating (Figure 4c), the samples are prepared on silicon wafers coated by electron-beam evaporation with a 5 nm chrome adhesion layer followed by a 75 nm gold layer. The gold-coated wafers are first immersed in a cationic solution of 3×10^{-3} poly (allylamine) hydrochloride (PAH) and 1 M NaCl for 5 min followed by immersion in an anionic solution of 3×10^{-3} M poly (styrenesulfonate) (PSS) and 1 M NaCl for 5 min. The samples are rinsed with a 1 M NaCl solution between successive layers. This process is repeated until the desired polymer thickness is obtained, with each bilayer having a ≈2 nm thickness. A top layer of PAH is then deposited to create a positively charged layer to promote nanocube adhesion.

The silver nanocubes were obtained from nanoComposix, Inc. (San Diego) in sizes ranging from 75 to 140 nm. The nanocubes are stored in ethanol and resuspended in water using centrifugation to a concentration of 3 mg mL^{-1} (corresponding to 3×10^{11} particles mL^{-1} for 100 nm nanocubes). To deposit 10 mm absorbers, a 5.5 µL droplet of the nanocube solution is deposited onto a 10 mm round cover glass, which is then inverted onto the polymer-coated sample. A 50 µm spacer is used to separate the cover glass and the sample to maintain uniform nanocube concentration across the region. The nanocube incubation time on the sample determines the final surface density (Figure 3). After the desired time, the nanocube solution is washed away and the sample is dried in nitrogen gas. For conformal coating (Figure 4), the samples were immersed completely into a diluted nanocube solution (0.1 mg mL^{-1}) and incubated for 8 h while stirring.

Optical Measurements: White light reflectance measurements at near normal incidence were carried out on a commercial spectrophotometer. Angle resolved reflectivity measurements (Figure 5) were done on a goniometer setup in which the angle of incidence and angle of collection could be independently controlled. The light source was a spectrally broad lamp with emission from the visible to the near-infrared. The reflected or scattered white light from the sample was collected via a fiber and spectrally resolved on a spectrograph with a silicon camera.

Supporting Information

Supporting Information is available from the Wiley Online Library or from the author.

Acknowledgements

G.M.A., J.H., T.B.H, and M.H.M. acknowledge support from the Air Force Office of Scientific Research Young Investigator Research Program (AFOSR, Grant. No. FA9550-15-1-0301). G.M.A. acknowledges support from the Intelligence Community Postdoctoral Research Fellowship Program. P.T.B. and D.R.S. acknowledge support from the Air Force Office of Scientific Research (Contract No. FA9550-12-1-0491).

Received: July 7, 2015
Revised: September 12, 2015
Published online:

[1] H. A. Atwater, A. Polman, *Nat. Mater.* **2010**, *9*, 205.
[2] W. Li, J. Valentine, *Nano Lett.* **2014**, *14*, 3510.
[3] B. Zhang, J. Hendrickson, J. Guo, *J. Opt. Soc. Am. B* **2013**, *30*, 656.

[4] X. Liu, T. Tyler, T. Starr, A. F. Starr, N. M. Jokerst, W. J. Padilla, *Phys. Rev. Lett.* **2011**, *107*, 045901.
[5] N. Liu, M. Mesch, T. Weiss, M. Hentschel, H. Giessen, *Nano Lett.* **2010**, *10*, 2342.
[6] J. J. Talghader, A. S. Gawarikar, R. P. Shea, *Light Sci. Appl.* **2012**, *1*, e24.
[7] Y. Cui, Y. He, Y. Jin, F. Ding, L. Yang, Y. Ye, S. Zhong, Y. Lin, S. He, *Laser Photonics Rev.* **2014**, *8*, 495.
[8] C. Wu, B. Neuner, G. Shvets, J. John, A. Milder, B. Zollars, S. Savoy, *Phys. Rev. B* **2011**, *84*, 075102.
[9] N. I. Landy, S. Sajuyigbe, J. J. Mock, D. R. Smith, W. J. Padilla, *Phys. Rev. Lett.* **2008**, *100*, 207402.
[10] D. O. Sigle, L. Zhang, S. Ithurria, B. Dubertret, J. J. Baumberg, *J. Phys. Chem. Lett.* **2015**, *6*, 1099.
[11] Z. P. Yang, L. Ci, J. A. Bur, S. Y. Lin, P. M. Ajayan, *Nano Lett.* **2008**, *8*, 446.
[12] A. Y. Vorobyev, C. Guo, *Phys. Rev. B* **2005**, *72*, 195422.
[13] C. Wu, C. H. Crouch, L. Zhao, J. E. Carey, R. Younkin, J. A. Levinson, E. Mazur, R. M. Farrell, P. Gothoskar, a. Karger, *Appl. Phys. Lett.* **2001**, *78*, 1850.
[14] M. A. Kats, R. Blanchard, P. Genevet, F. Capasso, *Nat. Mater.* **2012**, *12*, 20.
[15] K. Aydin, V. E. Ferry, R. M. Briggs, H. A. Atwater, *Nat. Commun.* **2011**, *2*, 517.
[16] C. M. Watts, X. Liu, W. J. Padilla, *Adv. Mater.* **2012**, *24*, OP98.
[17] X. Ni, N. K. Emani, A. V. Kildishev, A. Boltasseva, V. M. Shalaev, *Science* **2012**, *335*, 427.
[18] N. Yu, P. Genevet, M. a Kats, F. Aieta, J.-P. Tetienne, F. Capasso, Z. Gaburro, *Science* **2011**, *334*, 333.
[19] A. Silva, F. Monticone, G. Castaldi, V. Galdi, A. Alù, N. Engheta, *Science* **2014**, *343*, 160.
[20] T. V. Teperik, F. J. García de Abajo, A. G. Borisov, M. Abdelsalam, P. N. Bartlett, Y. Sugawara, J. J. Baumberg, *Nat. Photonics* **2008**, *2*, 299.
[21] A. Moreau, C. Ciracì, J. J. Mock, R. T. Hill, Q. Wang, B. J. Wiley, A. Chilkoti, D. R. Smith, *Nature* **2012**, *492*, 86.
[22] A. Tittl, P. Mai, R. Taubert, D. Dregely, N. Liu, H. Giessen, *Nano Lett.* **2011**, *11*, 4366.
[23] Z. Fang, Y.-R. Zhen, L. Fan, X. Zhu, P. Nordlander, *Phys. Rev. B* **2012**, *85*, 1.
[24] R. Walter, A. Tittl, A. Berrier, F. Sterl, T. Weiss, H. Giessen, *Adv. Opt. Mater.* **2015**, *3*, 398.
[25] M. K. Hedayati, M. Javaherirahim, B. Mozooni, R. Abdelaziz, A. Tavassolizadeh, V. S. K. Chakravadhanula, V. Zaporojtchenko, T. Strunkus, F. Faupel, M. Elbahri, *Adv. Mater.* **2011**, *23*, 5410.
[26] Z. Liu, X. Liu, S. Huang, P. Pan, J. Chen, G. Liu, G. Gu, *ACS Appl. Mater. Interfaces* **2015**, *7*, 4962.
[27] K. Liu, X. Zeng, S. Jiang, D. Ji, H. Song, N. Zhang, Q. Gan, *Nanoscale* **2014**, *6*, 5599.
[28] P. T. Bowen, D. R. Smith, *Phys. Rev. B* **2014**, *90*, 195402.
[29] J. B. Lassiter, F. McGuire, J. J. Mock, C. Ciracì, R. T. Hill, B. J. Wiley, A. Chilkoti, D. R. Smith, *Nano Lett.* **2013**, *13*, 5866.
[30] Q. Zhang, W. Li, L.-P. Wen, J. Chen, Y. Xia, *Chem. Eur. J.* **2010**, *16*, 10234.
[31] M. J. Rozin, D. A. Rosen, T. J. Dill, A. R. Tao, *Nat. Commun.* **2015**, *6*, 7325.
[32] M. L. Brongersma, N. J. Halas, P. Nordlander, *Nat. Nanotechnol.* **2015**, *10*, 25.
[33] X. Li, D. Xiao, Z. Zhang, *New J. Phys.* **2013**, *15*, 023011.
[34] R. Sundararaman, P. Narang, A. S. Jermyn, W. A. Goddard III, H. A. Atwater, *Nat. Commun.* **2014**, *5*, 5788.
[35] C. Ciraci, A. Rose, C. Argyropoulos, D. Smith, *J. Opt. Soc. Am. B* **2014**, *31*, 2601.
[36] Q.-Y. Lin, Z. Li, K. a. Brown , M. N. O'Brien, M. B. Ross, Y. Zhou, S. Butun, P.-C. Chen, G. C. Schatz, V. P. Dravid, K. Aydin, C. A. Mirkin, *Nano Lett.* **2015**, *15*, 4699,
[37] Y. Sun, Y. Xia, *Science* **2002**, *298*, 2176.